Synthesis and analysis of silver–copper alloy nanoparticles of different ratios manifest anticancer activity in breast cancer cells

Sara Al Tamimi, Sarmadia Ashraf, Tahir Abdulrehman, Aijaz Parray, Said A. Mansour, Yousef Haik, Shahnaz Qadri

Al Tamimi *et al. Cancer Nano* (2020) 11:13
https://doi.org/10.1186/s12645-020-00069-1

Cancer Nanotechnology

RESEARCH Open Access

Synthesis and analysis of silver–copper alloy nanoparticles of different ratios manifest anticancer activity in breast cancer cells

Sara Al Tamimi[1], Sarmadia Ashraf[1], Tahir Abdulrehman[1], Aijaz Parray[2], Said A. Mansour[3], Yousef Haik[4] and Shahnaz Qadri[4*]

*Correspondence: Sqadri@hbku.edu.qa
[4] College of Science and Engineering, Hamad Bin Khalifa University, Doha, Qatar
Full list of author information is available at the end of the article

Abstract

Background: Breast cancer is therapeutically very challenging to treat as it has the main four known genetic alterations, which result in the existence of several phenotypes leading to the difference in the mode of therapy and with poor outcome. Metallic nanoparticles of silver or copper have been studied previously as anticancer agents in breast cancer and other types of cancers. However, the anticancer effect of silver–copper alloy nanoparticles (AgCu-NP) is not studied in breast cancer. In this study, we aim to synthesize silver nanoparticles (Ag-NP), or copper nanoparticles (Cu-NP), and AgCu-NP and evaluate their toxicity in breast cancer and healthy breast cells.

Results: We synthesized sodium citrate and mercapto-propionic acid (MPA-3) capped water-soluble metallic nanoparticles of Ag-NP or Cu-NP and an alloy of three different combinations of AgCu-NP. High-resolution transmission electron microscopy characterization of nanoparticles revealed the spherical shape nanoparticles of varied sizes, furthermore dynamic light scattering characterization was performed, which investigated the hydrodynamic size and stability in phosphate buffer solution. Energy-dispersive X-ray spectroscopy (EDS) measurements were obtained from the transmission electron microscope to study the composition of alloy nanoparticles and the distribution pattern of silver and copper in the alloy nanoparticles. We measured the toxicity of nanoparticles to breast cancer MCF-7 cell line by MTT assay and compared the toxic effect with non-cancerous breast epithelial cells MCF-10A. Our data showed that Ag-NP or Cu-NP have no effect on cancer cells or healthy cells, except Ag-NP at 20 µg/ml were toxic to cancer cells. However, AgCu-NP were significantly toxic to MCF-7 cells at 10 µg/ml concentration, while as AgCu-NP have no toxic effect on healthy cells. Furthermore, we observed the cell death pathway by the apoptosis marker Annexin-V which showed non-significant results, while the exposure of AgCu-NP in MCF-7 cells leads to toxicity and also caused significant increase in MMP-9 level, which suggests the cell death may be associated with other pathways such as autophagy and oxidative stress related.

Conclusion: The data suggest that the AgCu-NP alloy imposes preferential toxicity in breast cancer MCF-7 cells and thus could be exploited as a new candidate for further anticancer investigation

Keywords: Silver nanoparticles, Copper nanoparticles, Anticancer activity, Breast cancer, Lung cancer, Silver–copper alloy

Background

Breast cancer is considered as one of the leading causes of death in women worldwide (Bray et al. 2018). The standard treatments for breast cancer include surgery, radiation, chemotherapy, hormone therapy, targeted therapy, and immunotherapy. However, there are limitations in conventional treatments, such as resistance, reoccurrence, metastasis, cytotoxicity to healthy cells (Curigliano and Criscitiello 2014; Kumari et al. 2016; MAYO CLINIC 2018; Tang et al. 2013). Improvements in chemotherapy have progressed since the introduction of monoclonal antibody therapy or Antibody Drug conjugates (ADC), which has the least toxicity compared to chemotherapy; however, monoclonal antibody therapy or ADC is showing drug resistance, and 40% of patients have shown relapse (Kahl et al. 2019; McLaughlin et al. 1998). By the emergence of nanotechnology, the biological properties such as the antimicrobial, antifungal, and anticancer activity of Ag-NP and Cu-NP are widely studied because of inexpensive and easy approachable methods of synthesis (Din and Rehan 2017; Roy et al. 2019).

The current use of Ag-NP in the medical field is for wound treatment, burns, disinfectants, and the development of orthopedic implants (Burdușel et al. 2018). Besides, Ag-NP are widely studied for their antimicrobial activity against a broad range of bacterial species (Le Ouay and Stellacci 2015). Also, the anticancer activity of Ag-NP tested in several forms of cancers (Bethu et al. 2018; Gurunathan et al. 2018). Similarly, Cu-NP extensively studied for antimicrobial activity, and recently antiviral and anticancer activity of Cu-NP is also reported (Nagajyothi et al. 2017; Yugandhar et al. 2017). Synergistic effect of Silver and copper nanoparticles embedded in chitin has shown enhanced toxicity in MCF-7 cancer cells comparing to Ag-NP or Cu-NP; this suggests that the formation of the AgCu-NP alloy may be a potent anticancer agent for MCF-7 breast cancer (Solairaj et al. 2017).

Based on previous findings of anticancer properties of Ag-NP and Cu-NP, we aim to synthesize AgCu-NP alloy nanoparticles, which may exhibit synergistic modality as a potent anticancer agent against MCF-7 cancer.

In this study, we aim to synthesize AgCu-NP as an anticancer agent and assess their cytotoxic effects in MCF-7 breast cancer. In this work, Ag-NP, Cu-NP, and three alloys of AgCu-NP of varying concentrations of silver and copper are chemically synthesized. The synthesized nanoparticles characterized for their shape and size using an electronic transmission microscope (TEM) and their hydrodynamic size and stability assessed by dynamic light scattering (DLS) and zeta potential. The semi-quantitative chemical analysis of nanoparticles was performed by energy-dispersive spectroscopy (EDS) to determine silver or copper and the ratio of silver and copper among alloy nanoparticles. MTT assay was employed to measure the toxicity in cancer and healthy cells caused by nanoparticle's exposure to find the lethal toxic dose. Also, toxicity in cells caused by nanoparticles was further assessed for the Apoptotic pathway and the regulation of metalloprotease enzymes, which are crucial in the cell death pathway (Kessenbrock et al. 2010; Yadav et al. 2020). The possible mechanism of toxicity lead by Ag-NP or Cu-NP is mainly by oxidative stress, DNA damage and lipid peroxidation, involving apoptosis or

autophagy cell death pathway. However, the mechanism that drives to cell death pathway by nanoparticles is still unknown (Aziz et al. 2019; Bernstock et al. 2016; Bethu et al. 2018; Yugandhar et al. 2017; Zielinska et al. 2018).

Results

Nanoparticle characterization

The high-resolution TEM images of the synthesized nanoparticles showed spherical shaped particles of different sizes. Also, lattice fringes were visualized in the nanoparticles, which is a characteristic of having a crystalline form, as shown in Fig. 1. The average diameter of synthesized AgCu-NP varied with silver or copper composition, the smallest size among AgCu-NP was 70:30 (Ag:Cu) percent, as shown in Table 1. The nanoparticles with the largest diameter were among the Ag-NP, which were synthesized by the sodium borohydride method. In contrast, Cu-NP, and all three combinations of AgCu-NP were synthesized by the hydrazine hydrate protocol. To check the nanoparticle's stability, the Zeta potential and hydrodynamic sizes were measured in phosphate buffer saline, as listed in Table 1. The Zeta potentials of Ag-NP, Cu-NP, and AgCu-NP (70:30) were more than − 50 mV, predicting better stability in aqueous solution. The nanoparticles, AgCu-NP (Ag:Cu, 50:50) and AgCu-NP (Ag:Cu, 30:70), showed a Zeta potential of − 27.9 and − 29.4 mV, respectively, considered as moderate stability in aqueous solution. This difference in Zeta potential among nanoparticles could be due to the composition of the

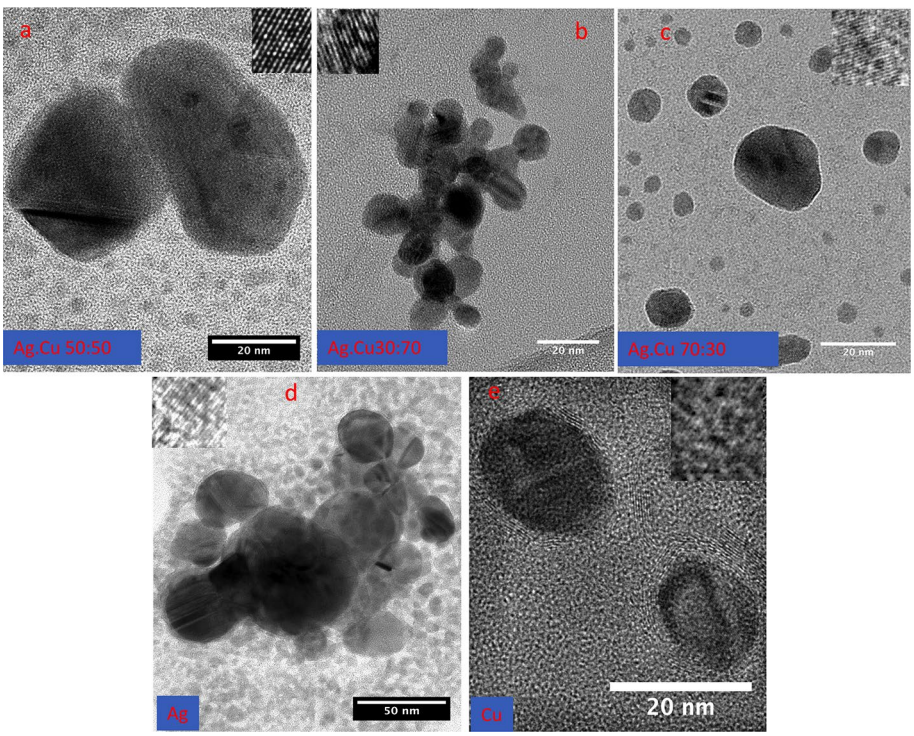

Fig. 1 TEM images: Nanoparticles of Ag-NP, Cu-NPr, or alloys of Ag–Cu-NP. Three types of alloyed particles were synthesized by adding the following concentrations of Silver and copper: 50:50, 30:70, and 70:30, as shown in figures **a**, **b**, and **c**, respectively. The silver and copper nanoparticles are shown in figures **d** and **e**, respectively

Table 1 Characterization of Nanoparticles which shows the surface charge as zeta potential, hydrodynamic size by DLS, and average size by TEM imaging

	Zeta potential mV	DLS nm	TEM Nm
Ag-NP	− 68.6 STDEV = 5.04	49.35 STDEV = 13.8 PDI = 0.281	7–31
Cu-NP	− 50.7 STDEV = 4.46	6.0 STDEV = 1.13	6–14
AgCu-NP 50:50	− 27.9 STDEV = 4.34	147 STDEV = 40 PDI = 0.541	20–32
AgCu-NP 70:30	− 51 STDEV = 6.11	9.5 STDEV = 2.3 PDI = 0.594	5–11
AgCu-NP 30–70	− 29.4 STDEV = 8.21	3.15 STDEV = 0.85 PDI = 0.594	4–20

nanoparticles; however, the reason for AgCu-NP to be more stable needs to be studied further. The hydrodynamic sizes of nanoparticles are generally higher than the TEM measurements, as shown in Table 1 and are relatively in close range of the TEM measurements.

EDS spectral maps identified silver and copper in all groups of the synthesized nanoparticles and shown in Fig. 2. The composition of AgCu-NP obtained from EDS analysis, as summarized in Table 2, showed the approximate ratio of silver and copper present in AgCu-NP (50:50), AgCu-NP (70:30), and AgCu-NP (30:70). To map the distribution of silver and copper in the AgCu-NP, we used Scanning transmission electron microscopy (STEM-EDS) and High-angle annular dark-field (HAADF) images, as shown in Fig. 3. The silver and copper EDS maps of AgCu-NP of all three compositions showed the homogenous distribution of Ag and Cu. Also, sulfur blended in all three compositions of AgCu-NP, which is due to the capping agent MPA-3 used during synthesis. Oxygen was abundant, it may be from the organic ligands such as MPA-3 and trisodium citrate used in synthesis. However, the oxygen in the EDS could be from the metal oxides as well.

Cell toxicity

In this study, we evaluated the anticancer effect of Ag-NP, Cu-NP, and the combination of AgCu-NP alloy nanoparticles. Besides their anticancer effect, we assessed their toxic effect on normal breast epithelial cells (MCF10-A cell line). MTT cell proliferation assay of MCF7 and MCF10A cell toxicity observes a dose-dependent exposure of nanoparticles. The nanoparticles showed significant toxicity in MCF-7 cells in comparison to MCF-10A, as shown in Fig. 4. The Ag-NP and Cu-NP did not show substantial toxicity in MCF-7 or MCF10A, except Ag-NP at 20 μg/ml were toxic to cancer cell line MCF-7. All three combinations of AgCu-NP showed up to a 50% decrease in viability of cancer cells when treated with varying concentrations of nanoparticles from 5 to 20 μg/ml; however, AgCu-NP 70:30 showed moderate toxicity in healthy cells (MCF10A) as well. Additionally, we did MTT assay in lung cancer NCI-1975 cells. Results show that

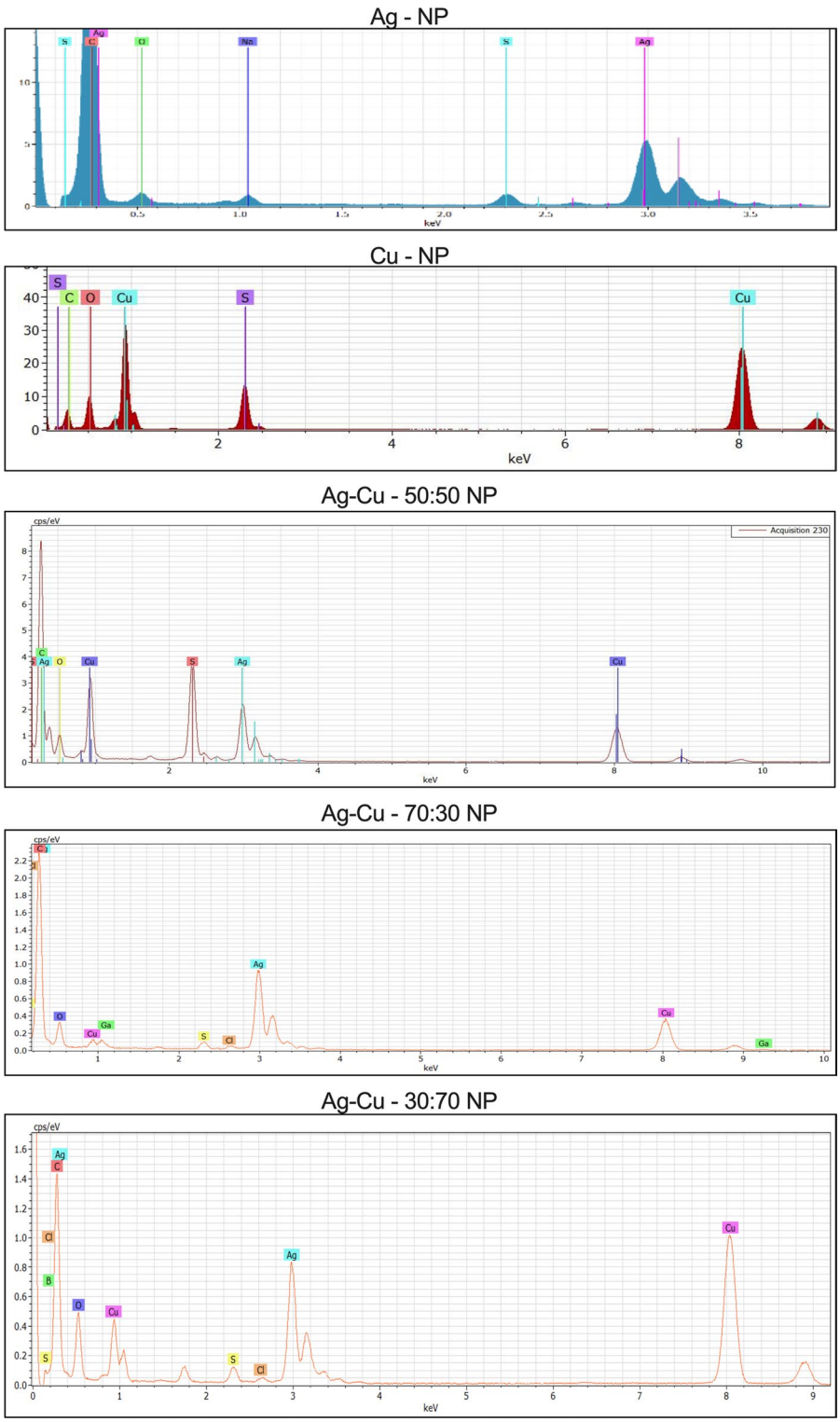

Fig. 2 EDS spectra of nanoparticles. The silver and Copper spectral peaks identified in EDS spectroscopy, as shown in figures, represent Ag-NP, Cu-NP, AgCu-NP 50:50, AgCu-NP 70:30, AgCu-NP 30:70

Table 2 Chemical composition of AgCu-NP by EDS spectroscopy, shows the elemental composition in synthesized AgCu-NP nanoparticles

Element	Series	(norm.wt%)	(norm. at.%)
AgCu 50:50			
Sulfur	k-series	14.06	9.39
Carbon	k-series	43.84	78.20
Copper	k-series	13.09	4.41
Silver	L-series	27.05	5.37
Oxygen	k-series	1.96	2.63
AgCu 70:30			
Oxygen	k-series	3.86	18.24
Copper	k-series	22.50	26.76
Gallium	L-series	0.68	0.74
Silver	L-series	71.04	49.76
Sulfur	k-series	1.86	4.39
Chlorine	k-series	0.05	0.11
AgCu 70:30			
Oxygen	k-series	4.33	17.09
Boron	k-series	0.92	5.35
Copper	k-series	48.33	48.00
Silver	L-series	44.68	26.14
Sulfur	k-series	1.69	3.32
Chlorine	k-series	0.05	0.09

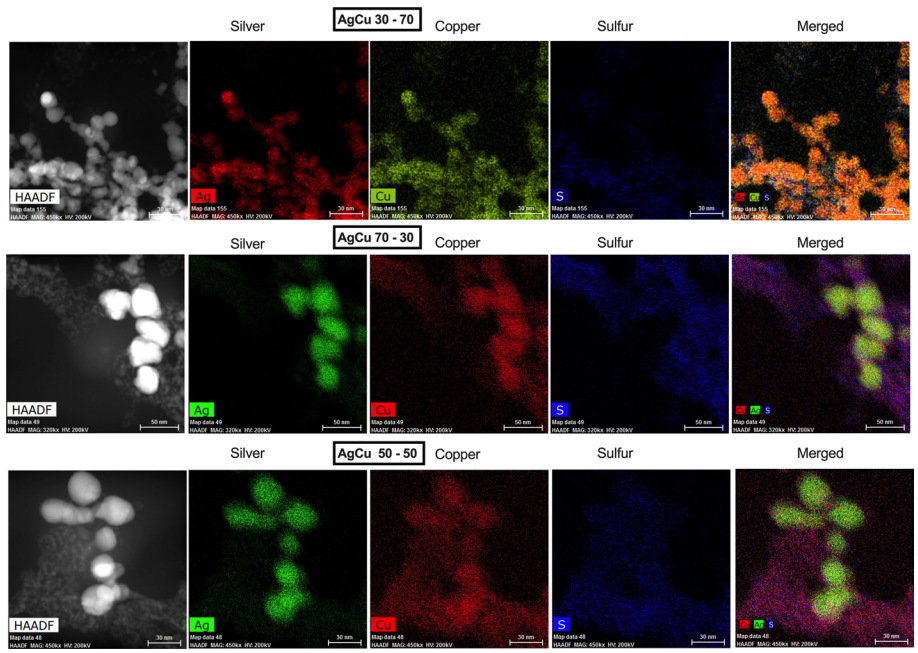

Fig. 3 EDS mapping of Ag and Cu in three alloyed compositions of, AgCu 30:70, AgCu 70:30, AgCu 50:50 showed Ag and Cu are alloyed

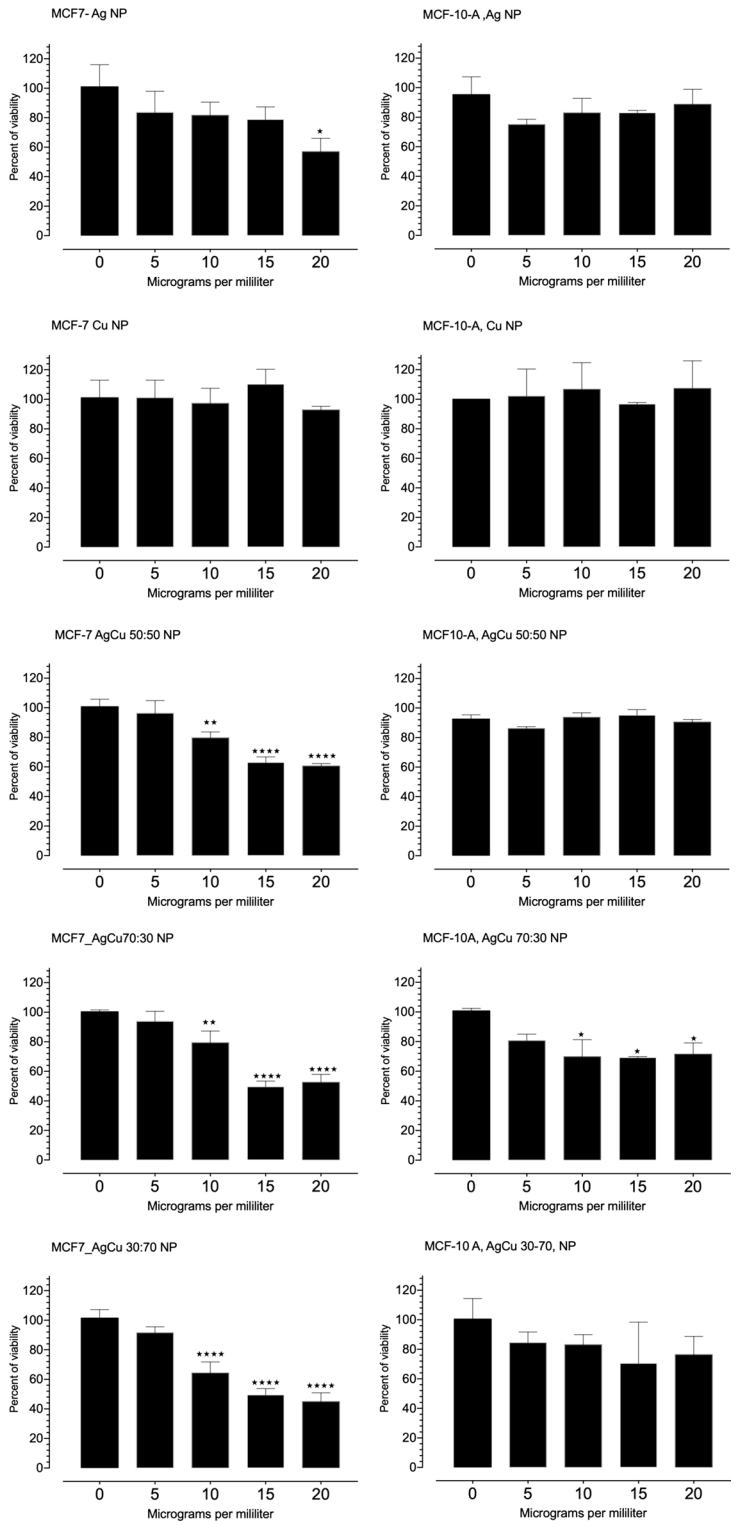

Fig. 4 MTT assay, Normal, and cancerous cells treated with nanoparticles were incubated for 48 h. Each bar represents the mean value of triplicates ± standard deviation. The significance test p values > 0.0001 represented as ****

AgCu-NP possesses toxicity in lung cancer cells, as shown in Additional file 1: Figure S1. Data showed that Ag-NP or Cu-NP had no significant toxicity in lung cancer cells, while AgCu-NP of all three combinations were significantly toxic to Lung cancer cells. MCF-7 breast cancer and NCI-1975 lung cancer are two different forms of cancers by their mode of action. Our data showed a toxic impact of synthesized nanoparticles (Ag-NP, Cu-NP, AgCu-NP) against cancer cells and healthy cells, among which AgCu-NP showed preferential toxicity in cancer cells.

To check if the apoptosis pathway is involved in MCF-7 by AgCu-NP 70:30, we tested the Annexin-V marker and propidium iodide (PI) staining. Our results showed no significant staining in early or late apoptosis in both the MCF-7 or MCF10A cells, as shown in Fig. 5, while PI-stained cells increased by 20%, as shown in the bar graph in Fig. 5. These data suggest that other mechanisms may involve the cell death pathway. To prove the toxic effect of AgCu-NP, we also run apoptosis assay in lung cancer NCI-1975 cells, and there was a significant difference in early and late apoptosis stages comparing to control, as shown in Additional file 1: Figure S2. Our data also suggest that toxicity may involve different cell death pathways among different types of cancer cells. In this study, our interest is MCF-7 breast cancer because of its more prevalent cause of death in women.

Several metals are essential at the metabolic level for the enzyme activity. Among the family of proteases, metalloproteases have crucial role in cell toxicity. To measure the effect of AgCu-NP 70:30 on metalloprotease enzymes, we analyzed MMP9 and MMP2 in MCF-7 and MCF10A cells, as shown in Fig. 6. Our results demonstrated that MMP-9 was significantly upregulated in MCF-7 cancer cells and remained unaffected in healthy MCF10A cells. The AgCu-NP in MCF-7 cells caused expression on MMP-9 significantly comparing to MCF10A cells, while MMP-2 remain unaffected by exposure of AgCu nanoparticles in both cancer and healthy cells.

Discussion

Significant work has been done on the synthesis, design, and application of metallic Ag-NP and Cu-NP nanoparticles in diagnostics and therapeutic values due to their unique physical and chemical properties (Azharuddin et al. 2019; Lombardo et al. 2019; Wei et al. 2015). The significant physio-chemical properties of nanoparticles that determine their biological interactions include size, shape, charge, agglomeration, dissolution and surface capping. In this work, we synthesized Ag-NP, Cu-NP, and three compositions of AgCu-NP by similar methods described earlier (Abdulrehman et al. 2020). This reaction is identical to one-pot nanoparticle synthesis, following the nucleation and growth by LaMer and coworkers. The reaction time (mixing of salts and reducing agents) was 3 h until the dark brown-reddish color was formed, and nanoparticles were harvested. However, to check if nanoparticle's growth may increase, we let the reaction continue for 24 h. The size, shape, and yield of AgCu-NP did not alter (data not shown). Here, the factors limiting size of nanoparticles may also be by capping agents MPA-3 and trisodium citrate, and the reducing rate of precursor metal salts. If the concentration of precursor atoms drops below the minimum super-saturation level, no further nucleation is possible; the same applies to the growth of our AgCu-NP (Xia et al. 2009). However, the detailed mechanism that controls the growth and size of the AgCu-NP with different percentages of silver and copper is unknown and needs to be studied further.

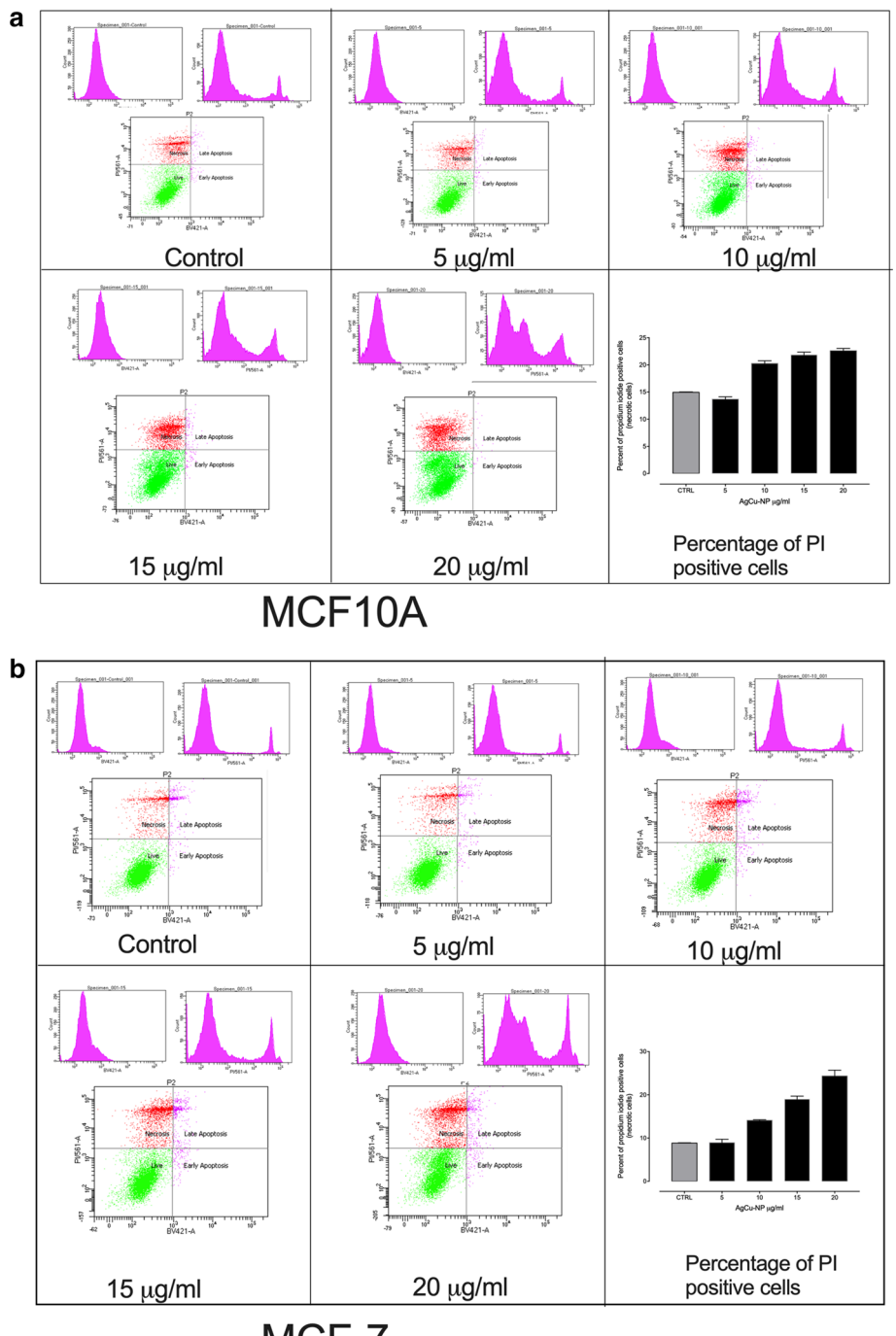

Fig. 5 Flow cytometry of Annexin-V and PI dye. The (A) and (B) shows the Annexin-V Bv421 and propidium iodide in the flow cytometry analysis of MCF10A and MCF-7 cells. The bar graphs plotted for the values obtained from PI dye (propidium iodide staining) as a measure of necrotic cells in MCF-7 and MCF-10A cells treated with Ag–Cu 70:30 alloy nanoparticles. Each bar represents the mean ± standard deviation

The nanoparticle characterization was initially carried by measuring hydrodynamic sizes and zeta potential, which confers the nanoparticle stability and average size. These data also suggest that nanoparticles in phosphate buffer remained stable and did not

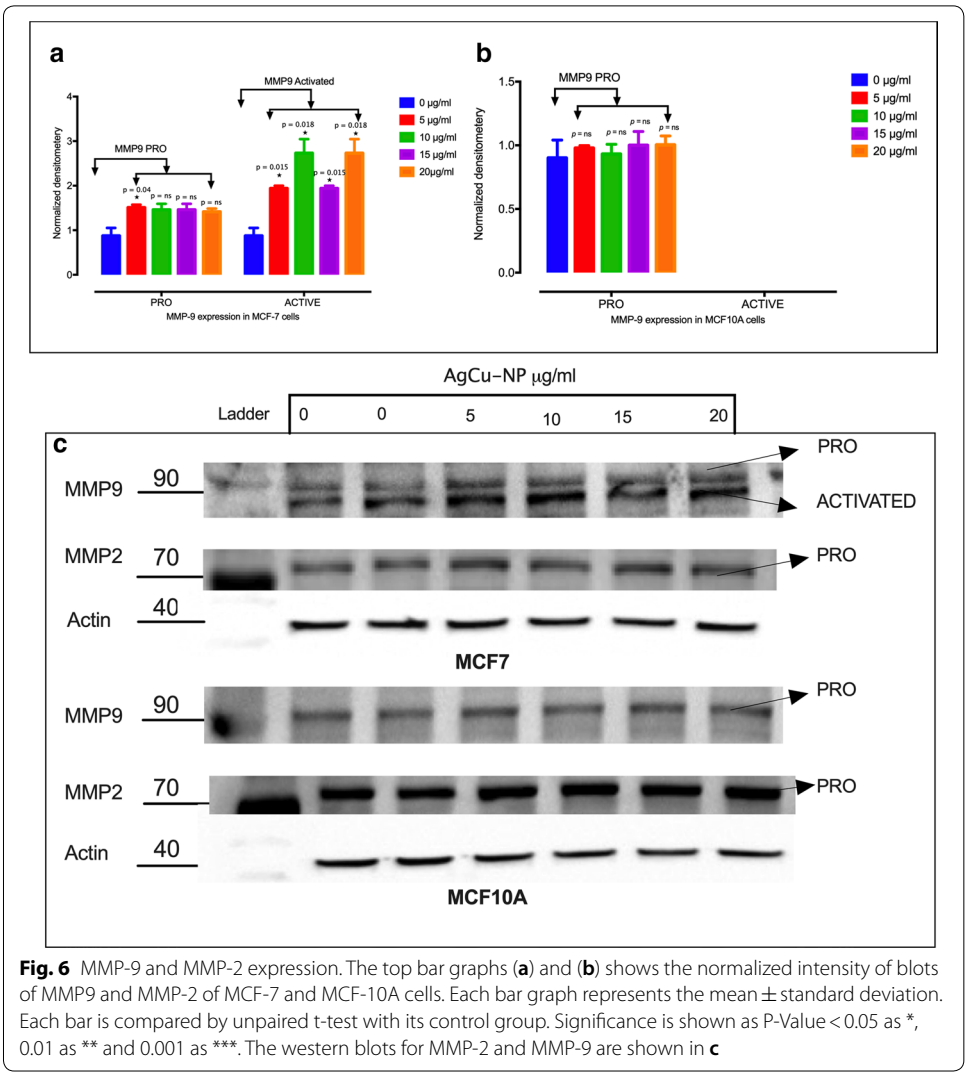

Fig. 6 MMP-9 and MMP-2 expression. The top bar graphs (**a**) and (**b**) shows the normalized intensity of blots of MMP9 and MMP-2 of MCF-7 and MCF-10A cells. Each bar graph represents the mean ± standard deviation. Each bar is compared by unpaired t-test with its control group. Significance is shown as P-Value < 0.05 as *, 0.01 as ** and 0.001 as ***. The western blots for MMP-2 and MMP-9 are shown in **c**

agglomerate. Furthermore, TEM and EDS characterization confirmed the elemental composition of AgCu-NP in Fig. 1. The composition of AgCu-NP in three combinations with molar ratios of Ag:Cu salts were as 70:30, 30:70, and 50:50, and their corresponding EDS data calculated from normalized atomic weight percent are as shown in Table 2. EDS maps of AgCu-NP showed a homogenous distribution of silver and copper within a nanoparticle. The distribution of sulfur in AgCu-NP by EDS maps supports the capping of nanoparticles by MPA-3.

We proceed to measure the toxicity of nanoparticles by MTT assay; this assay measures mitochondrial dehydrogenase enzyme. There are reports which mention nanoparticles can interfere with soluble formazan complex formed at the intracellular level of the WST-1 reagent, which is an analog of MTT reagent. Hence, we use conventional MTT assay, which forms insoluble formazan complex within the cells. The spectrophotometric measurements are obtained in pure DMSO reagent rather than cell culture media. MTT reagent has been widely used for measuring Ag-NP or Cu-NP toxicity. Our results show that significant toxicity was seen in cancer cells by AgCu-NP comparing to Ag-NP

or Cu-NP; however, AgCu-NP only 70:30 showed mild toxicity in healthy cells, as shown in Fig. 4.

Furthermore, we tested MTT assay in another type of cancer, lung cancer NCI-1975, as shown in Additional file 1: Figure S1, which indicates that AgCu-NP was toxic to lung cancer cells similar to MCF-7 cells. Overall, this work showed the significant selective toxicity in cancer cells comparing to healthy cells. However, a mechanism that kills only cancer cells is unknown. The cancer cells are indefinitely fast-dividing and metabolically more active than normal cells, which results in high production and consumption of ATP (Kim 2018). Cancer cells produce higher levels of superoxides, hydroxyl radicals, and hydrogen peroxide. Paradoxically, there is upregulation of antioxidants in cancer cells that enhances metabolic activity and growth in cancer cells (Panieri and Santoro 2016). Hence, we hypothesize that Ag and Cu ions in cancer cells have a higher chance of interacting with hydrogen peroxide at the intracellular level in cancer cells. Ag and Cu ions may react with hydrogen peroxide and form hydroxyl radicals, which is a deadly toxic molecule, till now, there is not any known antioxidant to detoxify the hydroxyl radicals. Future studies will be interesting to study the mechanism of AgCu-NP-mediated cytotoxicity in breast cancer cells involving oxidative stress.

In our previous work, we have deeply studied the toxicity of AgCu-NP in vitro and in animal studies which showed that AgCu-NP above 20 μg/ml are toxic in healthy cells, and above 2 mg/kg of body weight in animals showed inflammatory response by IL 1b and IL 6 and danger signal S100A9, also showed the mechanism of AgCu-NP-induced inflammation by the NLRP3 inflammasome. Hence, we aim to study AgCu-NP toxicity in cancer cells, which are safe in healthy cells; otherwise, it may be impossible to translate our research in future clinical studies (Ramadi et al. 2016).

Next, we tested if apoptosis is a cause of cell death; however, our Annexin-V results were non-significant, and PI staining, which counts for dead cells, increased by 20%. While lung cancer showed Annexin-V-positive staining indicated the role of apoptosis, these data reflect that cell death in MCF-7 could be initiated by other pathways such as oxidative stress, autophagy, and necrosis. The oxidative stress lead cell death is usually associated with Autophagy (Filomeni et al. 2015).

Furthermore, metalloproteases (MMPs) are linked to cell death pathways. MMPs have been widely studied for its role in tissue remodeling, inflammation, and cancer invasion. However, it is more complicated than it is to believe concerning the degradation of the extracellular matrix by MMPs. Instead, it controls the signaling pathways in the normal physiological process in healthy and diseased cells (Kessenbrock et al. 2010). However, its role varies in different cells such as in macrophages, whereas MMP-9 is packaged directly into vesicles with support of microtubules without taking part in the autophagy–lysosomal pathway in a pathological process (Hanania et al. 2012). It is worth noting that the function of MMPs varies drastically in two metastatic breast cancer cells MDA-MB-231 and MDA-MB-435. The antitumor drug *sodium phenylacetate* increased the intracellular level of MMP-9 and MMP-1 in MDA-MB-435. While as secretion of MMP1 and MMP-9 was increased in MDA-MB-23 and the formation of auto-phagosomes were seen which further suggests that the regulation of MMPs in breast cancer takes part in autophagic cell death and or apoptosis in MDA-MB-231 (Augustin et al. 2009).

It was recently shown that the role of MMP-9 in hyperglycemia-induced cell death in human cardiac stem cells showed MMP-9 initiates apoptosis irrespective of hyperglycemia and determines MMP-9 upstream to SAPK/JNK signaling and demonstrated MMP-9-mediated apoptosis. This study also reveals that MMP-9 is upstream to MAP/JNK signaling and plays a major role in hyperglycemia-induced ROS generation in human cardiac stem cells (Yadav et al. 2020). Briefly, MMP-9 has a pivotal role in cell survival.

In this work, our data showed that MCF-7 cells with the exposure of AgCu-NP upregulated the expression of MMP-9; however, it remains unchanged in non-cancerous MCF10A cells. Hence, these data suggest that further study is needed to determine the mechanism of toxicity in MCF-7 cells mediated by AgCu-NP and the role of MMP-9 in toxicity, which could give a new insight into cancer therapy. We have studied the toxicity of AgCu-NP in animals and have predicted the safe and toxic doses when administered sub-dermally or intravenously. Further studies in animal cancer models will explore the feasibility of using the AgCu-NP at known sub-lethal doses for cancer therapy.

Conclusion

The nanoparticle synthesis in this work is an environmentally friendly method to obtain alloyed AgCu-NP, which possess more potent anticancer activity than Ag-NP or Cu-NP nanoparticles. Our findings suggest that AgCu-NP alloyed nanoparticle selectively increased toxicity in cancer cells and did not affect normal cells. The role of AgCu-NP's in cell toxicity is not fully understood; we suggest that future work is needed to unveil the role of oxidative stress and MMP-9 in cytotoxicity caused by AgCu-NP in MCF-7 cells.

Materials and methods

Synthesis of silver nanoparticles

Ag-NP were prepared in 25 ml of degassed water by mixing 10 mM of each salt; silver nitrate, mercaptopropionic acid, and sodium hydroxide, the solution was kept under vigorous mixing. The mixture of the solution was added dropwise in 20 ml of degassed water containing 10 mM of sodium borohydride and 10 mM of sodium citrate with vigorous shaking using a magnetic stirrer at 4 °C. In 3 h, suspension turn in to orange to red color. The reaction was stopped by adding cold acetone to precipitate nanoparticles. Furthermore, nanoparticles were obtained by centrifugation at 4000 *g* for 10 min. Particles were re-suspended in 70% ethanol for washing and collected by centrifugation, and finally, particles were re-suspended in deionized water and centrifuged to collect the pellet. Nanoparticle pellet was flash-frozen with liquid nitrogen and kept for freeze-drying, and powder form was obtained and stored at − 80 °C for future use.

Copper nanoparticles

10 mM of salts containing copper acetate, mercaptopropionic acid, and sodium hydroxide was prepared in 25 ml of degassed water and were kept under mixing. The solution was added dropwise in 25 ml of degassed water containing 10 mM of hydrazine hydrate and sodium citrate. The reaction was continued under argon atmosphere with vigorously mixing for another 3–4 h until the solution turns to dark red color. Particles were obtained as a dry powder similar to Ag-NP's procedure, as mentioned earlier.

Silver–copper alloy

AgCu-NP (50:50), AgCu-NP (70:30), and AgCu-NP (30:70) alloy nanoparticles were prepared similar to Cu-NP protocol, except the ratio of silver or copper salt was added according to the combination of Ag and Cu. Each batch was obtained as a freeze-dried powder and stored in − 80 °C temperature.

Characterization of nanoparticles.

The freeze-dried powder was dissolved in deionized water and sonicated. The sample for TEM imaging was prepared by depositing a small drop of diluted solution onto Lacy/Carbon thin film on a copper grid and allowed to evaporate and dry at room temperature. Images were obtained high-resolution transmission electron microscopy (HRTEM) using FEI TALOS X operated at 200 kV, coupled with superX EDS detector.

The size, crystallinity, and elemental analysis of nanoparticles were obtained by transmission electron microscopy (TEM) and energy-dispersive X-ray spectroscopy (EDS). The EDS confirmed the presence of silver or copper in the five compositions of nanoparticles; (AgCu-NP 70:30), (AgCu-NP 30:70), (AgCu-NP 50:50), (Ag-NP) and (Cu-NP).

Furthermore, particle size and zeta potential were measured using Zeta sizer nano Malvern (ZSP), and graphs were generated by software (Zetasizer). The average size of particles was obtained from TEM images by using Fiji software.

MCF-7 and MCF 10-A cell culture

MCF-7 breast cancer cell line and MCF-10-A breast normal cell line were grown in DMEM cell culture media with high glucose-containing L-glutamine (2 mM), 10% Fetal bovine serum (FBS), penicillin and streptomycin 100 U/ml (Gibco by Life Technologies—15140-122). The cells were grown in the incubator at 37 °C under a humidified atmosphere containing 5% CO_2.

Cell cytotoxicity (MTT assay)

Cells were seeded onto 96-well cell culture plates at a cell density of 1×10^5 cells/well. After 24 hr of incubation, fresh DMEM high glucose media with L-glutamine (2 mM), 10% Fetal bovine serum (FBS), penicillin, and streptomycin 100 U/ml. Varying concentrations (5, 10, 15, and 20 μg/ml) of Ag-NP, Cu-NP, and or different alloyed compositions of AgCu-NP were added to cells growing on 96-well plates and were incubated for 48 h. Following incubation, MTT (Thermo Fisher Scientific V13154) assay was performed as directed by the supplier's protocol. After incubation time, media were aspirated slowly, and 50 μL of Dimethyl sulfoxide (DMSO) was added to each well and incubated for 15 min to dissolve insoluble formazan crystals. The absorbance of the formazan dye was read at 540 nm using a TECAN-SPARK plate reader.

Flow cytometry-based cell apoptosis assay

Annexin-V-BV421 (Brilliant Violent 421 Annexin-V; Biolegend) and Propidium Iodide was used to evaluate apoptosis and necrosis. MCF-7 or MCF-10A cells were seeded

in six-well culture plate (50,000 cells/well). After 24 h, fresh media was fed containing AgCu-NP (70:30) of varying concentrations ranging from 5 to 20 µg/ml and incubated for 48 h. The group of cells without nanoparticle treatment was considered as a negative control. Annexin staining was performed as directed by the manufacturer's protocol. Briefly, post-incubation cells were washed with 1 mL of phosphate-buffered saline (PBS), and 700 µL of Accutase cell dissociation buffer was added and kept for 5–10 min in the incubator. Then, added 2 mL of fresh media and cells were collected by centrifugation at 1000 rpm for 5 min. The cell pellet was re-suspended in 500 µL of 1 × binding buffer of Annexin-V-BV421 and 5 µL of propidium iodide was added, followed with incubation at room temperature for 5–10 min in the dark. The stained cells were analyzed by flow cytometer using FACS Calibur (BD LSRFortessa).

MM-2 and MMP-9 expression level by western blot

MCF-7 and MCF-10-A cells were plated individually in a six-well culture plate. After 24 h of incubation, changed the DMEM media in a final volume of 2 mL and treated cells with AgCu(70:30) nanoparticles with varying concentrations (5, 10, 15, and 20 µg/ml). After 48 h of treatment, cells were washed with 1 mL of phosphate-buffered saline (PBS) and 700 µL Accutase cell dissociation buffer was added and kept for 5–15 min in the CO_2 incubator. 2 mL of fresh media containing 10% serum was added, then cells were harvested by centrifugation at 1000 rpm for 5 min. After that, the cell pellet was first washed with 1 mL of 1 × PBS for 5 min at 1000 *g*. Then, the cell pellet was re-suspended in pre-cooled lysis RIPA buffer containing proteinase inhibitors and incubated on ice for 30 min. The cell lysate was centrifuged at 8000 *g* to remove the cell debris. The supernatant was transferred and stored on ice. The sample was mixed with 2× Laemmli buffer (161-0737-Bio Rad) mixed thoroughly, followed by heating at 95 °C for 10 min. 5 mM of 2-Mercaptoethanol (161–0710-Bio Rad) was added to the denatured lysate, and 50 µg of denatured protein from each sample was loaded in the precast 10% SDS-PAGE (4561033EDU – Bio RaD), and electrophoresis was carried at 100 V.

The protein was transferred to 0.2 µm PVDF membrane (Immun-Blot PVDF membranes—162-0177 Bio Rad) were pretreated with Tris-buffered saline containing 0.05% tween-20 (TBS-T) and 5% non-fat dry milk at room temperature for 2 h. The membranes were blocked for non-specific binding and incubated with Rabbit polyclonal primary anti-MMP-2 or MMP-9 antibody for overnight at 4 °C. Primary antibody dilutions were used as anti-MMP-2 1:500 (ab37150—Abcam) and Anti-MMP-9 1:1000 (ab38898—Abcam). Following primary antibody incubation, blots were washed three times in TBST buffer and secondary antibody (Polyclonal Goat Anti Rabbit IgG, HRP conjugated (Millipore Cat.No. 12-348) in 1:5000 dilution was incubated for one hour, and substrate (Western ECL 170-5061—Bio Rad) was added. Clarity and Chemi Doc System was used for obtaining images.

Supplementary information

Supplementary information accompanies this paper at https://doi.org/10.1186/s12645-020-00069-1.

Additional file 1: Figure S1. Lung cancer MTT assay. **Figure S2.** Annexin-V and PI staining in Lung cancer cells.

Abbreviations
Ag-NP: Silver nanoparticles; Cu-NP: Copper nanoparticles; AgCu-NP: Silver–copper nanoparticles; MMP-9: Metalloprotease enzyme 9; MMP-2: Metalloprotease enzyme 2; MTT: 3-(4,5-Dimethylthiazol-2-yl)-2,5-diphenyltetrazolium bromide.

Acknowledgements
We are thankful to Ms. Sajitha V.P. at the Interim Translational Research Institute (iTRI), Hamad Medical Corporation, Qatar, for her assistance provided in western blot experiments. We also like to thank Dr. Siveen Sivaraman for his support in Flow cytometry at the core lab of iTRI, Hamad Medical Corporation. We also Acknowledge Dr. Shahab Uddin Khan at iTRI, Hamad Medical Corporation, for providing NCI-1975, MCF10A and MCF-7 cell lines. The publication of this article was funded by the Qatar National Library.

Authors' contributions
All authors have made significant contributions to work discussed in this manuscript. ST, SA and TA performed the experiments and did the analysis, SQ, AP, SM and YH designed the experiments and analyzed the data. YH, SA, SM prepared the manuscript. All authors revised the final manuscript. All authors read and approved the final manuscript.

Funding
This work was supported by the Department of Sustainability, College of Science, Hamad Bin Khalifa University. In addition, the publication of this paper was funded by the Qatar National Library.

Availability of data and materials
All data generated or analyzed during this study are included in this published article.

Ethics approval and consent to participate
Not applicable.

Consent for publication
Not applicable.

Competing interests
The authors declare that they have no competing interests in this article.

Author details
[1] College of Health and Life Sciences, Hamad Bin Khalifa University, Doha, Qatar. [2] Neuroscience Institute, Hamad General Hospital, Doha, Qatar. [3] Qatar Environment and Energy Research Institute, Hamad Bin Khalifa University, Doha, Qatar. [4] College of Science and Engineering, Hamad Bin Khalifa University, Doha, Qatar.

Received: 29 January 2020 Accepted: 15 November 2020
Published online: 25 November 2020

References

Abdulrehman T, Qadri S, Skariah S, Sultan A, Mansour S, Azzi J, et al. Boron doped silver-copper alloy nanoparticle targeting intracellular *S. aureus* in bone cells. PLoS ONE. 2020;15(4):e0231276.
Augustin S, Berard M, Kellaf S, Peyri N, Fauvel-LAFÈVE F, Legrand C, et al. Matrix metalloproteinases are involved in both type I (Apoptosis) and type II (Autophagy) cell death induced by sodium phenylacetate in MDA-MB-231 breast tumour cells. Anticancer Res. 2009;29(4):1335–43.
Azharuddin M, Zhu GH, Das D, Ozgur E, Uzun L, Turner APF, et al. A repertoire of biomedical applications of noble metal nanoparticles. Chem Commun R Soc Chem. 2019;55(49):6964–96.
Aziz N, Faraz M, Sherwani MA, Fatma T, Prasad R. Illuminating the anticancerous efficacy of a new fungal chassis for silver nanoparticle synthesis. Front Chem. 2019;7:65.
Bernstock JD, Lee YJ, Peruzzotti-Jametti L, Southall N, Johnson KR, Maric D, et al. A novel quantitative high-throughput screen identifies drugs that both activate SUMO conjugation via the inhibition of microRNAs 182 and 183 and facilitate neuroprotection in a model of oxygen and glucose deprivation. J Cereb Blood Flow Metab. 2016;36(2):426–41.
Bethu MS, Netala VR, Domdi L, Tartte V, Janapala VR. Potential anticancer activity of biogenic silver nanoparticles using leaf extract of Rhynchosia suaveolens: an insight into the mechanism. Artif Cells Nanomed Biotechnol. 2018;46(1):104–14.
Bray F, Ferlay J, Soerjomataram I, Siegel RL, Torre LA, Jemal A. Global cancer statistics 2018: GLOBOCAN estimates of incidence and mortality worldwide for 36 cancers in 185 countries. CA Cancer J Clin. 2018;68(6):394–424.
Burdușel AC, Gherasim O, Grumezescu AM, Mogoantă L, Ficai A, Andronescu E. Biomedical applications of silver nanoparticles: an up-to-date overview. Nanomaterials. 2018;8(9):681.
MAYO CLINIC. Chemotherapy for breast cancer—Mayo Clinic. 2018. https://www.mayoclinic.org/tests-procedures/chemotherapy-for-breast-cancer/about/pac-20384931.
Curigliano G, Criscitiello C. Successes and limitations of targeted cancer therapy in breast cancer. Prog tumor Res. 2014;41:15–35.
Din MI, Rehan R. Synthesis, characterization, and applications of copper nanoparticles. Anal Lett. 2017;50:50–62.
Filomeni G, De Zio D, Cecconi F. Oxidative stress and autophagy: The clash between damage and metabolic needs. Cell Death Differ. 2015;22(3):377–88.
Gurunathan S, Qasim M, Park C, Yoo H, Kim JH, Hong K. Cytotoxic potential and molecular pathway analysis of silver nanoparticles in human colon cancer cells HCT116. Int J Mol Sci. 2018;19(8):2269.
Hanania R, Sun HS, Xu K, Pustylnik S, Jeganathan S, Harrison RE. Classically activated macrophages use stable microtubules for matrix metalloproteinase-9 (MMP-9) secretion. J Biol Chem. 2012;287(11):8468–83.

Kahl BS, Hamadani M, Radford J, Carlo-Stella C, Caimi P, Reid E, et al. A phase I study of ADCT-402 (loncastuximab tesirine), a novel pyrrolobenzodiazepine-based antibody–drug conjugate, in relapsed/ refractory B-cell non-Hodgkin lymphoma. Clin Cancer Res. 2019;25(23):6986–94.
Kessenbrock K, Plaks V, Werb Z. Matrix metalloproteinases: regulators of the tumor microenvironment. Cell. 2010;141(1):52–67.
Kim SY. Cancer energy metabolism: shutting power off cancer factory. Biomol Ther. 2018;26(1):39–44.
Kumari P, Ghosh B, Biswas S. Nanocarriers for cancer-targeted drug delivery. J Drug Target. 2016;24(3):179–91.
Le Ouay B, Stellacci F. Antibacterial activity of silver nanoparticles: a surface science insight. Nano Today. 2015;10(3):339–54.
Lombardo D, Kiselev MA, Caccamo MT. Smart nanoparticles for drug delivery application: development of versatile nanocarrier platforms in biotechnology and nanomedicine. J Nanomater. 2019.
McLaughlin P, Grillo-López AJ, Link BK, Levy R, Czuczman MS, Williams ME, et al. Rituximab chimeric anti-CD20 monoclonal antibody therapy for relapsed indolent lymphoma: half of patients respond to a four-dose treatment program. J Clin Oncol. 1998;16(8):2825–33.
Nagajyothi PC, Muthuraman P, Sreekanth TVM, Kim DH, Shim J. Green synthesis: in-vitro anticancer activity of copper oxide nanoparticles against human cervical carcinoma cells. Arab J Chem. 2017;10(2):215–25.
Panieri E, Santoro MM. ROS homeostasis and metabolism: a dangerous liason in cancer cells. Cell Death Dis. 2016;7(6):e2253.
Ramadi KB, Mohamed YA, Al-Sbiei A, Almarzooqi S, Bashir G, Al Dhanhani A, et al. Acute systemic exposure to silver-based nanoparticles induces hepatotoxicity and NLRP3-dependent inflammation. Nanotoxicology. 2016;10(8):1061–74.
Roy A, Bulut O, Some S, Mandal AK, Yilmaz MD. Green synthesis of silver nanoparticles: Biomolecule-nanoparticle organizations targeting antimicrobial activity. RSC Adv. 2019.
Solairaj D, Rameshthangam P, Arunachalam G. Anticancer activity of silver and copper embedded chitin nanocomposites against human breast cancer (MCF-7) cells. Int J Biol Macromol. 2017;105(1):608–19.
Tang X, Cai S, Zhang R, Liu P, Chen H, Zheng Y, et al. Paclitaxel-loaded nanoparticles of star-shaped cholic acid-core pla-tpgs copolymer for breast cancer treatment. Nanoscale Res Lett. 2013;8(1):1–12.
Wei L, Lu J, Xu H, Patel A, Chen ZS, Chen G. Silver nanoparticles: synthesis, properties, and therapeutic applications. Drug Discov Today. 2015;20(5):595–601.
Xia Y, Xiong Y, Lim B, Skrabalak SE. Shape-controlled synthesis of metal nanocrystals: simple chemistry meets complex physics? Angew Chemie Int Ed. 2009;48(1):60–103.
Yadav SK, Kambis TN, Kar S, Park SY, Mishra PK. MMP9 mediates acute hyperglycemia-induced human cardiac stem cell death by upregulating apoptosis and pyroptosis in vitro. Cell Death Dis. 2020;11:186.
Yugandhar P, Vasavi T, Uma Maheswari Devi P, Savithramma N. Bioinspired green synthesis of copper oxide nanoparticles from Syzygium alternifolium (Wt.) Walp: characterization and evaluation of its synergistic antimicrobial and anticancer activity. Appl Nanosci. 2017;7(7):417–27.
Zielinska E, Zauszkiewicz-Pawlak A, Wojcik M, Inkielewicz-Stepniak I. Silver nanoparticles of different sizes induce a mixed type of programmed cell death in human pancreatic ductal adenocarcinoma. Oncotarget. 2018;9(4):4675–97.

Publisher's Note